Proteolytically Stable Diaza-Peptide Foldamers Mimic Helical Hot Spots of Protein-Protein Interactions and Act as Natural Chaperones

Chenghui Shi,[a] Julia Kaffy,[a] Tâp Ha-Duong,[a] Jean-François Gallard,[b] Alain Pruvost,[c] Aloise Mabondzo,[c] Lidia Ciccone,[d] Sandrine Ongeri*[a] and Nicolo Tonali*[a]

[a] Université Paris-Saclay, CNRS, BioCIS, Bat. Henri Moissan, 17 av. des Sciences, 91400 Orsay, France, E-mail: sandrine.ongeri@universite-paris-saclay.fr and nicolo.tonali@universite-paris-saclay.fr

[b] Equipe Biologie et Chimie Structurales, Dept Chimie et Biologie Structurales et Analytiques, ICSN CNRS, Université Paris Saclay, 1 avenue de la terrasse, 91190 Gif sur Yvette, France

[c] Université Paris-Saclay, CEA, INRAE, Département Médicaments et Technologies pour La Santé, SPI 91191 Gif-sur-Yvette, France

[d] Department of Pharmacy, University of Pisa, 56126 Pisa, Italy

KEYWORD: Foldamer • peptidomimetic • azapeptide • helix • amyloid • cross-interaction • chaperone

ABSTRACT: A novel class of peptidomimetic foldamers based on diaza-peptide units is reported. Circular dichroism, ATR-FTIR, NMR, and Molecular Dynamics studies demonstrate that, unlike the natural parent nonapeptide, the specific incorporation of one diaza-peptide unit at the N-terminus allows helical folding in water, which is further reinforced by the introduction of a second unit at the C-terminus. The ability of these foldamers to resist proteolysis, to mimic the small helical hot spot of transthyretin-amyloid β (Aβ) cross-interaction and to decrease pathological Aβ aggregation, demonstrates that the introduction of diazapeptide units is a valid approach for designing mimics or inhibitors of protein-protein interaction and other therapeutic peptidomimetics. This study also reveals that small peptide foldamers can play the same role as physiological chaperone proteins and opens a new way to design inhibitors of amyloid protein aggregation, hallmark of more than 20 serious human diseases such as of Alzheimer's disease.

INTRODUCTION

Many biological processes are regulated through protein–protein interactions (PPIs) and the human interactome is believed to involve about 130,000–650,000 types of PPIs. However, aberrant PPIs are also associated with many human diseases such as cancer, infectious diseases, and neurodegenerative diseases.[1] The main challenge for medicinal chemists in targeting PPIs is the ability to mimic and modulate the large and relatively flexible surface areas of the hot-spots, i.e. peptide sequences located at PPIs.[1–3] The classical small molecules are generally not suitable for targeting PPIs. Therefore, research in this field has been oriented towards peptides, offering several advantages such as greater affinity, selectivity, and safety, owing to their intermediate size between small molecule drugs and protein therapeutics.[4] However, the major drawbacks of small peptides are their proteolytic instability and their low ability to adopt stable conformations, while PPI hot-spots generally involve well-defined secondary structures.[4,5] Peptidomimetic foldamers, mimicking bioactive conformations, represent a pharmacologically interesting class of compounds to target PPIs, as they are inspired by the structural features of their bioactive peptide counterparts, overcoming the drawbacks of natural peptide.[5,6] This field of foldamers has recently emerged as promising for the discovery of next generation drug candidates,[7,8] or as recognition elements for a potential use in diagnostic applications.[9]

However, to date only a few examples of foldamers presenting proteolytic stability, water solubility, flexibility of functionalities, solid-phase synthesis and efficiency in targeting PPIs have been reported. Two major works by Gellman[10] and Guichard[11] groups using α/β and oligourea peptides respectively can be cited as pioneering examples. We report here a novel class of foldamers based on diaza-peptide units and natural α-residues, showing water solubility, great stability towards proteolysis in human serum, and notable blood-brain barrier (BBB) permeability. We demonstrate that the helical propensity of this type of foldamers allows them to mimic secondary structures of proteins involved in PPI hot-spots.

The substitution of the α–CH of one amino-acid residue by a nitrogen atom has already provided biologically active peptides, such as Goserelin approved for the treatment of prostate cancer and having an aza-Gly residue at its C-terminus.[12–16] However, the introduction of two or more aza-amino acids in peptide sequences has not been studied both for the influence on the induced conformational properties and for the potential as biologically active peptidomimetic foldamers. We have recently developed the synthesis in solution of pseudotripeptides having two consecutive aza-amino acids,[17] and we demonstrated the formation of stable hydrogen-bonded β-turn structures of these units both in methanol and water.[18,19] A first pseudohexapeptide foldamer aza-Val/aza-Ala/α-Val/aza-Val/aza-Ala/α-Val was shown to adopt repeated β-turns conformations that interconvert with a fully helical structure mimicking a 3_{10} helix in methanol.[18] Here, we further

investigate the conformational propensities of longer foldamers having one, two or three diaza-peptide units in different positions and combinations.

As a proof of concept for the ability of this new class of foldamers to target PPIs, we selected the transthyretin (TTR)-β-amyloid (Aβ) interaction. TTR is a homo-tetrameric protein of 55 kDa, one of whose roles being to act as a natural chaperone protein of Aβ1-42 to inhibit its pathological aggregation.[20] Aβ aggregates still constitute one of the two major hallmarks of Alzheimer's disease (AD).[21–24] The protective role of TTR in AD has been confirmed by in vivo studies, in AD transgenic mice [25,26] and in AD patients where TTR concentration was observed to decrease both in plasma and CSF.[27,28] One key hotspot in TTR-Aβ interaction has been reported as the strand G in the inner TTR β-sheet (residues 102–117, Figure 1a).[29] Cyclic small peptides based on this strand G demonstrated to block Aβ1-42 in non-fibrillar aggregates.[30–32] Another TTR-Aβ hotspot has been recently mentioned with the demonstration that the EF-helix/loop (residues 74–83, Figure 1a) undergoes rearrangement in TTR crystals grown in the presence of Aβ1–28 and Cu^{2+}.[33] However, an EF-helix derived peptide had no effect on Aβ aggregate size and did not show significative interaction with Aβ, suggesting that the lack of α-helical structure of the isolated EF-helix peptide prevents its binding to Aβ.[29] In order to restore the EF helical conformation and thus its putative binding to Aβ, we report herein the design of a series of novel diaza-nonapeptide foldamers based on the sequence derived from the EF-helix (residues 75-83, Figure 1b) of TTR and the development of their synthesis by solid phase peptide synthesis (SPPS). The impact of the aza substitution in terms of number and position of residues on the secondary structure conformation in water, was evaluated using circular dichroism (CD), ATR-FTIR, NMR spectroscopy, and Molecular Dynamics (MD). Then, the ability of these azapeptides to interact with Aβ was assessed by studying the activity on Aβ conformation using CD, and on Aβ1-42 aggregation through Thioflavin T (ThT) fluorescence spectroscopy assays. Finally, the stability against proteolysis of the most promising foldamer and its ability to cross the BBB were evaluated.

RESULTS AND DISCUSSION

Design and Synthesis. We designed diaza-nonapeptide foldamers based on the sequence 75-83 of the EF-helix of TTR (Figure 1b, wild-type sequence 1) and compared both their conformational preferences and activities with the natural nonapeptide **1**, according to the number and the position of diaza-peptide units. The alkyl groups on the aza-amino acids were the exact mimics of the lateral chains of the natural α-amino acids Ala, Leu, Tyr and Lys or the homo-analogues for Trp and Thr. One diaza-amino acid unit was inserted at the C-terminus (**2**), in the middle (**3**) or at the N-terminus (**4**), or two diaza-peptide units were inserted in **5** (middle and C-terminus), **6** (N-terminus and middle), and **7** (N- and C-termini), or three units in all position (**8**). All the azapeptides were first acetylated at the N-terminus, and three of them were also prepared with a free terminal amine or hydrazine (**9**, **10** and **11**).

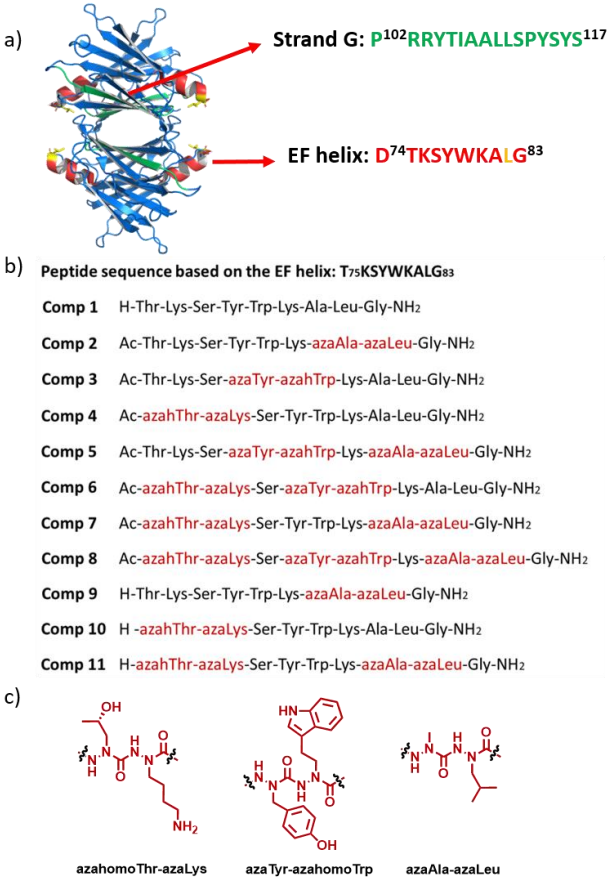

Figure 1. a) Representation of TTR tetramer (PDB entry 4PM1) highlighting the hot-spots of TTR- Aβ1-42 interaction (strand G in green and EF-helix in red, the Leu residue in the EF-helix crucial for the interaction is in yellow).[25] b) Representation of the natural peptide **1** (TTR 75-83) and of the designed foldamers bearing one (**2-4**), two (**5-7**) or three (**8**) diaza-amino acid units and three foldamers without acetyl group at the N-terminus (**9-11**). c) Structure of diaza-amino acid units.

The reference natural nonapeptide **1** was synthesized using classical Fmoc-based SPPS on the rink amide resin. For azapeptides **2-11**, a new SPPS protocol has been developed, by preparing the diaza-peptide building blocks **12-14** (Figure 2) in solution, according to our previously reported protocols [17,19] (Schemes S1-S3, SI), and by coupling them sequentially on solid support.

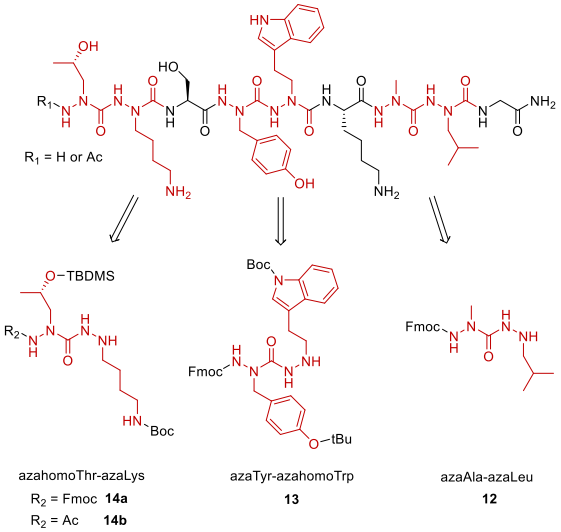

Figure 2. The building blocks designed for SPPS.

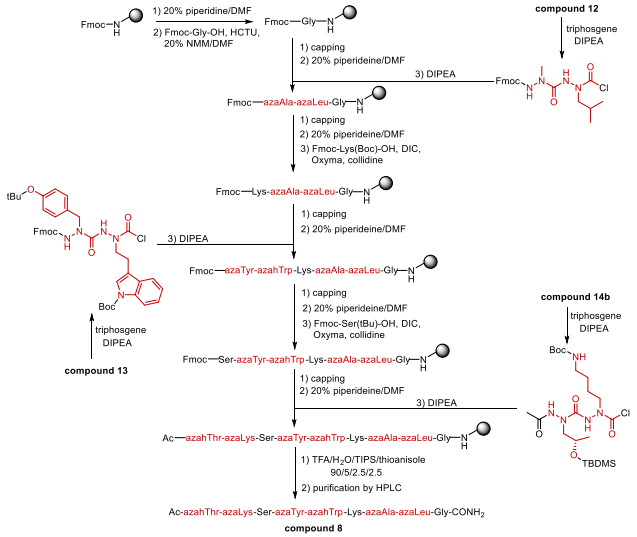

Scheme 1. SPPS strategy: synthesis of foldamer **8**.

The synthesis of different alkyl-hydrazide derivatives using reductive amination of various aldehydes with corresponding carbazates has been well demonstrated in literature.[34] AzahomoTrp was chosen instead of azaTrp because azaTrp is not stable in the acidic conditions used for the peptide cleavage from the resin (loss of an indolylmethyl moiety giving the aza-Gly).[35] We developed the synthesis of azahomoTrp precursor starting from 2-(1H-indol-3-yl)acetic acid that was reduced to aldehyde and reacted with Fmoc-hydrazine under reductive amination conditions (Scheme S2, SI). Because of synthetic issues, we used azahomoThr instead of azaThr to replace Thr in the sequence. Its synthesis was developed from S-ethylacetate that was protected, reduced in aldehyde and reacted with Fmoc or acetyl hydrazine under reductive amination conditions (Scheme S3, SI). The synthesis of diaza-nonapeptides on solid phase is illustrated for compound 8 in Scheme 1 as an example. The loading on the resin and the coupling between natural amino acids were performed using HCTU as coupling reagent in 20% (v/v) NMM/DMF. The diaza-peptide building blocks were introduced by activation using triphosgene in the presence of DIPEA for 15 min, prior to their addition to the resin and followed by the stirring of the mixture for 5h. To couple natural amino acids to resin-bound diaza-peptide fragments, we used DIC and Oxyma as coupling reagents and collidine as base. To afford the acetylated (**4** and **6-8**) or the free N-terminal (**10**, **11**) diaza-nonapeptides, units **14b** (with acetyl) and **14a** (with Fmoc) have been used respectively. All the final peptides were cleaved from the resin and protecting groups (Boc, TBDMS and tBu) were removed simultaneously using standard protocol (TFA/H2O/TIPS/thioanisole 95:5:2.5:2.5) and purified using semi-preparative HPLC. All the diaza-nonapeptides were obtained in satisfactory yields (7-15%).

Conformational studies by Circular dichroism, Infrared spectroscopy, Nuclear Magnetic Resonance spectroscopy and Molecular dynamics. CD analysis of all nonapeptides 1-11 was first performed in 20 mM phosphate buffer (PB). As expected, the natural peptide 1 showed a typically random coil conformation. Introducing a different number of diaza-peptides units at different positions in the sequence had dramatic impacts on the spectral shape. Compounds 2 and 4, which have one diaza-peptide unit at the C- or N-terminus respectively, showed a similar shape of CD spectrum with a strong negative band near 196 nm and a weak positive band near 225 nm, with 2 showing however a weaker positive band near 225 nm compared to 4 (Figure 3). Compound 7 and its non-acetylated analogue 11 which have two diaza-peptide units at the N- and C-termini showed a stronger positive band at 225 nm and a smaller negative band near 196 nm compared to 4 (Figure 3). When a diaza-peptide unit was inserted in the middle of the sequence (3, 5 and 6), the positive band near 225 nm disappeared and one maximum appeared near 210 nm (Figure S10, SI). When three diaza-peptide units were simultaneously present in the sequence (8, Figure S10, SI), the CD spectrum displayed one positive maximum between 190 nm and 200 nm and no negative band. These results underline that the introduction of diaza-peptide units at the *N*- and/or *C*-termini favors particular folded structures compared to random coil natural peptides, which are however destabilized by the introduction of the same motif in the middle of the sequence.

To our knowledge, a positive band near 225 nm has been reported in β/γ-peptides displaying 13-helix [36,37] or Aib foldamers showing right-handed 3_{10}-helix,[38,39] or in natural polyproline type II helix (PPII), but it is generally accompanied by a negative signal near 205 nm. In our case, PPII was excluded because this positive Cotton effect was only very modestly reduced at high temperature, slightly increased under high concentration of urea, and stable under $CaCl_2$ conditions (Figures S11-S13, SI).[40,41] The positive bands near 225 nm in the CD spectra of compounds **2**, **4**, **7** and **11** could also arise from the proximity of the two aromatic side chains of Tyr and Trp, [42,43] which may be a clue of a specific conformation allowing their proximity. Furthermore, a shift of the negative band towards 200 nm for the CD spectrum of 11 in ACN (Figure S14, SI), is in

accordance with an increased population of helical conformation, as found for 13-helix in β/γ-peptides,[36,37] or 3_{10}-helix in poly-Aib.[38,39]

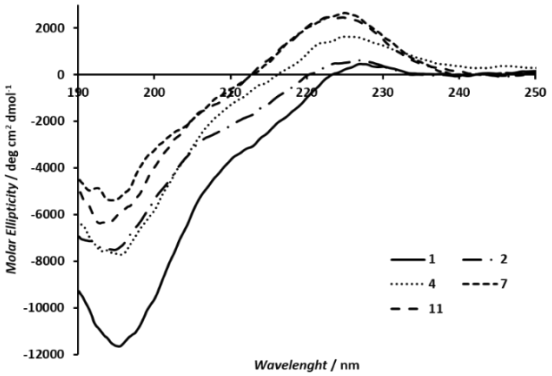

Figure 3. CD spectra of natural peptide **1** and foldamers **2**, **4**, **7** and **11** (125 μM in PB buffer, 37°C).

Thus, although CD analysis could not well define the structure of the azapeptides, it proved useful in selecting compounds **7** and **11**, showing the more pronounced helical structure, for further analysis using FTIR, NMR and molecular dynamics. In FTIR analysis, the amide I band (1600 – 1700 cm^{-1}) mainly originating from the peptide backbone CO stretching vibrations,[44] was deconvoluted to distinguish between the individual secondary structure types.[45] After evaporation from water, compound **7** showed 21% of β-turn and 16% of helix (α-/3_{10}) contents but also a significant amount of β-sheet (14% anti-parallel; 32% aggregated) and of unstructured conformations (17%) (Figure 4 A, C). Compound **11** showed a slightly different behavior adopting a stronger content of β-turn (35%) and helix (24%, α-/3_{10}-helices), with a smaller content of β-sheet in particular as aggregated strands (27% anti-parallel; 14% aggregated) and no random conformations (Figure 4 B, D). The high β-turn and helical contents are consistent with our previous results, which demonstrated that the sequential introduction of aza-amino acids induces repeated β-turns conformations, which can interconvert with a fully helical structure, mimicking a 3_{10}-helix.[18] Overall, **11** is more structured in β-turn/helical conformation than **7** that also exhibits a significant amount of unstructured and aggregated forms, the latter possibly due to lower solubility in water caused by the presence of the N-terminal acetyl group. Furthermore, the ratio between the α-helix (1650-1656 cm^{-1}) and 3_{10}-helix (1661-1664 cm^{-1}) contents (1.07 for **11** and 0.53 for **7**), indicates that **11** having a free N-terminal hydrazine appeared to explore a helical conformation in between α- and 3_{10}-helix, while **7**, due to the presence of the acetyl, changes its propensity towards a 3_{10}-helix.

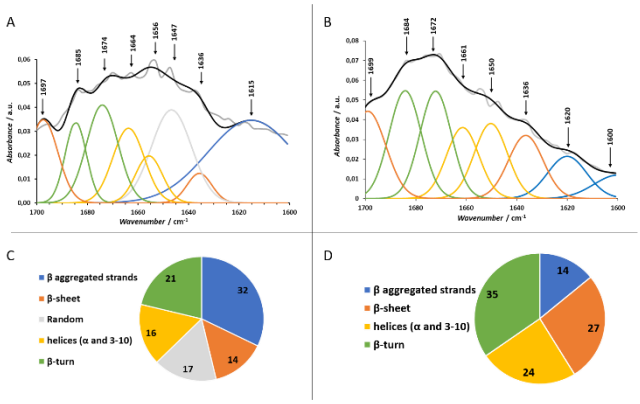

Figure 4. ATR-FTIR spectra of **7** (A) and **11** (B) dissolved in H2O (2 mM) and their corresponding deconvolution (C, D) for secondary structure quantification. Gray line: experimental curve; Black line: model curve curve (sum of the error squared 2.29 x 10^{-5} for **7** and 7.09 x 10^{-5} for **11**) after deconvolution. Averaged standard deviations: 7.25 for **7** and 7.09 for **11**.

Then, different NMR parameters were analyzed to assess the hydrogen bonding and folding propensities of compounds **7** and **11** in solution, in particular the temperature dependency of the amide proton chemical shift (temperature coefficient $\Delta\delta_{HN}/\Delta T$), vicinal $^3J_{HN\alpha}$ coupling constants and the through-space dipolar ^1H-^1H ROE correlations (for the detailed data, see SI). For compound **7**, in water, the fast exchange of amide protons resulted in the absence of signals for most of them at any temperature from 298 to 310 K, suggesting the absence of intramolecular hydrogen bonds (H-bond), and making difficult both the complete attribution of all signals and the calculation of temperature coefficient $\Delta\delta_{HN}/\Delta T$ and vicinal $^3J_{HN\alpha}$ coupling constants. Several ROEs between side chain protons and/or H_α and side chain protons of residues (*i*) and (*i+1*) have been observed (Ser[3]/Tyr[4], Trp[5]/Lys[6], Lys[6]/azaAla[7], Figures 5, S1 and S2, SI), as well as between residues (*i*) and (*i+3*) (Trp[5]/azaLeu[8], Figures 5, S1, S3, SI), suggesting a folded structure. Some ROEs between residues (*i*) and (*i+2*) have been also observed, however the similar chemical shifts of azaLys[2] and Lys[6] side chain protons prevent their unambiguous attribution (azaLys[2] or Lys[6]/ Tyr[4], Figure S1, SI). For compound **11** in water, all the amide NH resonances of natural residues and almost all the other proton chemical shifts pertinent for conformational analysis could be assigned at 310 K except for the amide NH of the aza-residues. The amide proton temperature coefficients from 298 to 310 K for residues Tyr (-6.0 ppb/K), Trp (-5.2 ppb/K) and Lys (-5.4 ppb/K) (Table S7, SI) were all below -4.5 ppb/K, indicating they were not involved in stable intramolecular H-bond. However, vicinal $^3J_{HN\alpha}$ coupling constants for the natural amino acids were observed with an average value of 5.7 ± 0,21 Hz (from 5.3 to 6.5 Hz, Table S7, SI), indicating preferred ϕ angle values in the -60° and -90° range, compatible with an helical folding.[46, 47]

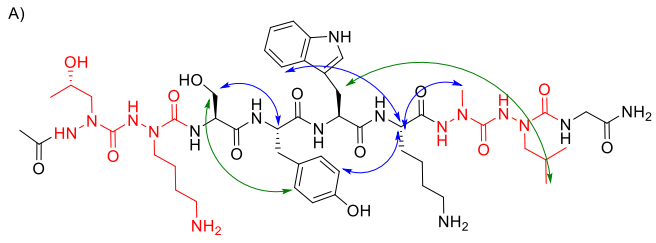

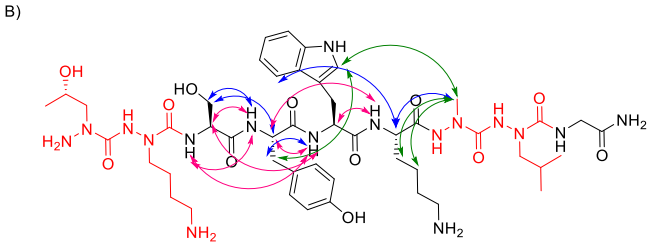

Figure 5. Structure of foldamers **7** (A) and **11** (B) in water showing the assigned ROEs: backbone-backbone in pink, backbone-side chain in blue, side chain-side chain in green.

Similar ROEs to those noted for **7** between side chain protons and/or H_α and side chain protons of residues (*i*) and (*i+1*) have been observed for **11** (Ser^3/Tyr^4, Trp^5/Lys^6, Lys^6/aAla^7) (Figures 5, S4-S6 SI). An additional ROE contact Tyr^4/Trp^5 and the absence of (*i*) and (*i+3*) Trp^5/azaLeu^8 contact suggest a slightly different folded structure compared to **7**, with a proximity between the side chains of these two aromatic central residues. It should be noticed also the presence of two characteristic 3_{10}-helical H_α/NH (*i*, *i+2*) ROEs (Ser^3/Trp^5 and Tyr^4/Lys^6, Figure S6, SI), and of two backbone NH-NH ROEs, one (*i*, *i+1*) between Ser^3 and Tyr^4 and one (*i*, *i+2*) between Ser^3 and Trp^5, all indicating a folded conformation in the central region of the peptide (Ser^3 to Lys^6). However, the fact that no intramolecular H-bonds could be observed might arise from the difficulty for **11** to maintain its H-bond network in water, due to the high solvation level. Thus, we decided to perform NMR analysis of compound **11** in DMF, which is an aprotic polar organic solvent favoring intramolecular H-bonds, in order to examine which amide protons might be involved in H-bond and if these H-bonds can support the folded structure found in water. Vicinal $^3J_{HN\alpha}$ coupling constants and ROEs parameters were calculated in DMF at 333 K, allowing the signals to be conveniently dispersed to perform the unambiguous attribution of all signals pertinent for the conformational analysis. Vicinal $^3J_{HN\alpha}$ coupling constants for the natural amino acids were observed with an average value of 6.3 ± 0.34 Hz (from 5.3 to 6.8 Hz, Table S7, SI), also compatible with a helical folding. Similar ROEs were found for **11** in DMF as those found in water, but additional long-range ROEs between residues (*i*) and (*i+3*) (azahThr^1/Tyr^4 and Ser^3/Lys^6) and between residues (*i*) and (*i+5*) (Ser^3/azaLeu^8) suggested a more folded structure of **11** in DMF (Figures S7- S9, SI). This suggestion was supported by the short-range ROE intensity ratios calculated for **11** in DMF (Table S8, SI). In fact, **11** in DMF showed N_α (*i*, *i*) / αN (*i-1*, *i*) ratios (sensitive to the value of the ψ angle of residue *i-1*) superior to 0,5, which is consistent with a shift to an increased population of helical backbone angles compared to these ratios in water.[48,49] Interestingly, in DMF, **11** showed a stronger propensity to form intramolecular H-bonds, as reflected by several small amide proton temperature coefficients between 298 and 333 K for residues Tyr^4(-3.8 ppb/K), Trp^5(-3.2 ppb/K), Lys^6(-3.5 ppb/K), Gly^9(-4.0 ppb/K) and for one of carboxamide protons (-1.9 ppb/K) (Table S7, SI).

In order to get more insights about the difference of **7** and **11**, and their ability to mimic the EF-helix of TTR, molecular dynamics (MD) analysis was conducted and the preferred structure of **7** and **11** was compared with EF-helix (see SI for more details).

Theoretical and experimental conformational ensembles of compounds **11** were compared by using the vicinal $^3J_{HN\alpha}$ coupling constants of its central natural amino acid segment Ser^3-Lys$_6$. The values calculated from its MD simulation are fairly close to those measured by NMR, with averaged values around 5.4-5.7 Hz (Table S9, SI) indicating that the backbone of the peptide central region has rather compact local conformations (<Φ> ~ -70°) in both experiments and simulations. This is confirmed by the computed Ramachandran plots of the two peptides indicating that the backbone dihedral angles (ϕ, ψ) of the central residues Ser^3 to Lys^6 predominantly have values of helical conformations (Figure S16, SI). The high propensity of both compounds **7** and **11** to form helical conformations during their MD simulations is illustrated in Figure 6, where it can be seen that the two most populated clusters of the two foldamers can be well superimposed on the α-helical segment 75-83 of TTR (see also videos in SI). It could be noted that along the MD simulation compound **7** rather engages (*i*, *i+3*) hydrogen bonds, characteristic of 3_{10}-helix, while 11 also engages (*i*, *i+4*) H-bonds, characteristic of α-helix (see the distributions of the computed backbone CO-HN H-bond lengths Figure S17, SI). By comparing the backbone (phi, psi) angles in the TTR EF-helix and in the two first clusters of compounds **7** and **11**, we confirmed that the central region of the 5 structures have (phi, psi) angles in the range of characteristic values of helical conformations (-60°, -50°) (Table S10, SI).

Regarding the orientations of the amino acid side chains, we observed few differences between simulations and NMR measurements (Figure S18, Tables S11-S13). Unlike MD, NMR indicate that Trp^5 is close to azaLeu^8 in **7** but close to Tyr^4 in **11**. Nevertheless, the proximity of Trp^5 and Tyr^4 side chains is observed in less populated clusters 2 of the simulated compounds **7** and **11.**

Compared to the crystallographic structure of TTR helix 75-83, the orientations of the amino acid side chains of compounds **7** and **11** are also not exactly the same (Figure 6). Indeed, in the most populated clusters 1 of both peptidomimetics, Trp^5 side chain is closer to Lys^6 than to Tyr^4 side chain, whereas the equivalent Trp^{79} in TTR helical segment is closer to Tyr^{78} than Lys^{80} side chain. However, unlike **7**, in both major clusters of **11**, the azaLeu^8 side chain is well oriented in the same direction as that of Leu^{82} of TTR (Table S14 and videos SI). This information could be important to note, as Leu^{82} has been reported as crucial to mediate TTR-Aβ interaction.[29]

Overall, these conformational analyses allowed us to establish that the specific incorporation of two diaza-peptide units at the N- and C-termini of nonapeptides provides the ability for these foldamers to adopt helical conformation even in water, although less hydrogen bonded and thus more flexible than in aprotic polar solvent. The presence or not of an acetyl group at the N-terminus in **7** and **11** respectively, slightly modifies the helical conformation (3_{10} for compound **7** and higher α-helical propensity for **11**) and the orientation of the side chains. Thus **11** seems to better mimic the crystallographic structure of TTR helix 75-83, as demonstrated by the better superimposition of their backbone as well as by the similar orientation of azaLeu^8 and the key Leu^{82} of TTR.

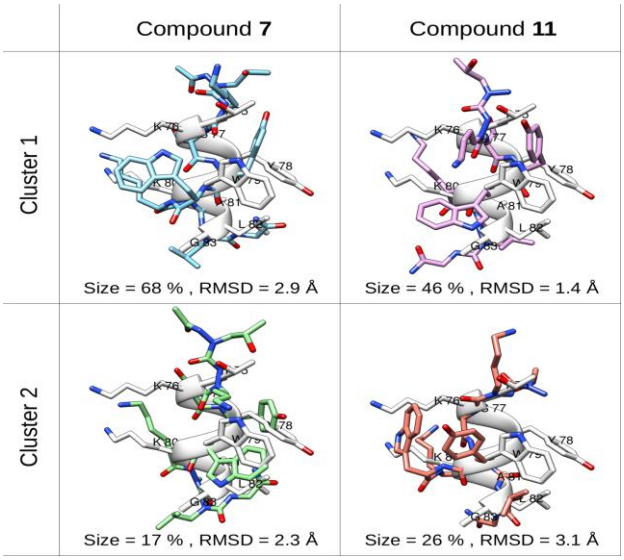

Figure 6. Representative structures of the two most populated clusters of compounds **7** (left) and **11** (right) superimposed on EF-helix (residues 75-83) of TRR PDB structure 5N7C (white). The size of each cluster is indicated as percentages of the MD trajectories. The RMSD are calculated over the C_α (or Nα) of the azapeptides.

Evaluation of amyloid aggregation inhibition. The next step was to evaluate the ability of our foldamers to mimic TTR-Aβ interaction and to have an impact on Aβ aggregation.

ThT fluorescence spectroscopy of Aβ1-42. We first performed Thioflavin-T (ThT) fluorescence assays to screen the activity of foldamers **2-11** on Aβ1-42 aggregation kinetics and compared it to that of the full length wt-TTR (as tetramer) and of the natural peptide **1** (representative curves are shown in Figure 7 and Figure S19, SI). ThT is a dye able to fluoresce upon binding to β-sheet rich structures [50] and it is the standard dye used to study the aggregation kinetics of amyloidogenic proteins.[51] The aggregation curve of Aβ1-42 alone displayed the classical sigmoidal pattern, characterized by 3 different portions: an initial lag phase of about 3h, followed by a rapid elongation phase which ends to a final plateau reached after about 10h (purple curves). The ability of the compounds to modulate Aβ1–42 aggregation was assessed considering the time of the half-aggregation ($t_{1/2}$) and the intensity of the experimental fluorescence plateau (F). No or small effect was observed at 1/1 ratio for peptides **1-11** (Table S15, SI). At 10/1 ratio, all the azapeptides **2-8** having an acetyl group at the N-terminus presented a similar decrease of the plateau (-30% < ΔF < -62%) but a weaker activity to delay Aβ42 aggregation (+30% < $\Delta t_{1/2}$ < +107%) compared to the effect of the natural peptide **1** and of TTR (ΔF=-59, -73% and $\Delta t_{1/2}$ = Δ209, 303% for **1** and TTR respectively, Table 1). However, the azapeptides **10** and **11**, having a free hydrazine at their N-terminus, reach similar efficiency to delay Aβ1-42 aggregation (ΔF=+193 and ΔF=+254% respectively) and decrease the fluorescence plateau (-54 and -59%). Notably, **10** and even more **11** possessing one or two diaza-peptide units at the N- or at the N- and C- terminus respectively, showed these interesting results, while compound **9** having one diaza-peptide unit at its C-terminus was much less active to delay the aggregation ($t_{1/2}$ =+36%). Thus, two diaza-peptide units at the N- and C- terminus induce stronger helical CD signals and higher activity on Aβ1-42 aggregation, than one diaza-peptide unit at the N-terminus and these effects are greatly reduced if the diaza-peptide unit is introduced at the C-terminus. However, while compounds **7** and **11** showed similar CD spectra, they showed dramatic difference in their anti-aggregation activity. We hypothesized that this difference comes from their small differences in helical conformation, reflecting a better superposition of **11** on the EF-helix of TTR, and/or from the presence or the absence of an acetyl group at the N-terminus. Indeed, the presence of the free hydrazine at the N-terminus can also provide an additional ionic interaction with Aβ1-42, supporting our previous observations on the importance of establishing ionic interactions with acidic residues of Aβ1-42 (E3-11-22, D1-7-23 or C-term of A42).[52-55]

AmyloFit. We next investigated the microscopic mechanisms underlying the inhibition of the process of Aβ1-42 amyloid fibril formation by the TTR-derived peptide **1** and foldamer **11** using AmyloFit.[56,57] Under our conditions, Aβ1-42 alone follows a molecular model in which the mechanism dominating the kinetics of aggregation is the secondary nucleation (Table S17, SI). The experimental data for TTR are consistent with predictions made by altering the rate constants of secondary nucleation (k_2) or elongation (k_+). The secondary nucleation pathway is specifically perturbed. In particular, the k_+k_2 value in the presence of TTR was found to decrease by a factor of approximately 100 and 10 with 10 μM and 2.5 μM TTR concentration, respectively. The same effect is observed for peptide **1**, with the k_+k_2 value decreased by a factor of 100 at 100 μM concentration (ratio 10/1, no effect observed at 1/1 ratio). Conversely, the experimental data for foldamer **11** are consistent with predictions made by altering the product of the rate constants of elongation and primary nucleation (k_+k_n), thus demonstrating that the primary nucleation pathway is specifically perturbed, by a factor of 10^9 at 100 μM (ratio 10/1), and 10 at 10 μM (ratio 1/1). This analysis showed a different mechanism of inhibition of our foldamer **11** compared to TTR and EF-helix derived peptide.

Table 1. Effects of compounds **1-11** and wt-TTR (tetramer) on $A\beta_{1-42}$ fibrillization assessed by ThT-fluorescence spectroscopy at 10/1 ratio of compound/$A\beta_{1-42}$ for **1-11** and 1/1 ratio of wt-TTR/$A\beta_{1-42}$.

Compound	$t_{1/2}$ extension (%)[b]	F reduction (%)[c]
1	+209±65%	−59±8%
2	+59±6%	−30±8%
3	+102±10%	−56±11%
4	+107±4%	−36±15%
5	+34±3%	−55±7%
6	+72±20%	−62±8%
7	+30±6%	−41±6%
8	+42±2%	−41±6%
9	+36±7%	−60±5%
10	+193±30%	−54±6%
11	+254±90%	−57±2%
wt-TTR	+303±11%	−73±2%

Parameters are expressed as mean ± SE, n=3. [a] Compounds were dissolved in water. The concentration of Aβ1-42 was 10 μM. [b] See supporting information for the calculation of the $t_{1/2}$ extension. [c] See supporting information for the calculation of the F reduction.

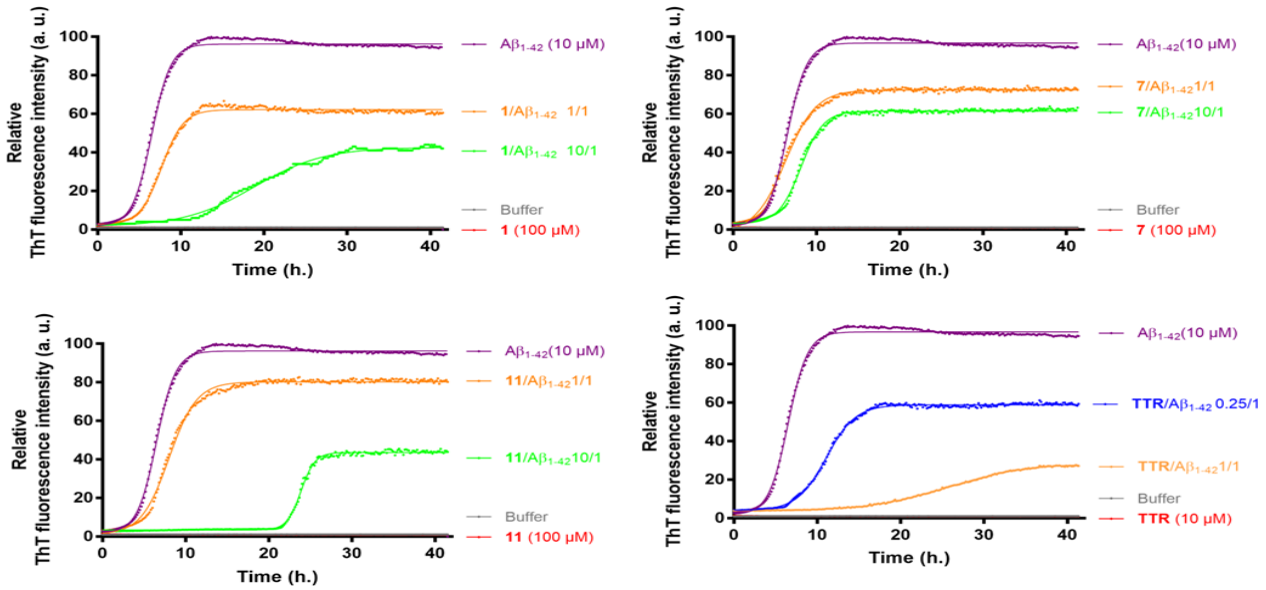

Figure 7. Representative curves of Tht fluorescence assays over time showing Aβ1-42 aggregation (peptide at 10 μM, Tht at 40 μM, room temperature, 10 sec of 600 rpm double orbital shaking before the first cycle only) in the absence (purple curve) and in the presence of compounds **1**, **7**, **11** and wt-TTR (tetramer) at compound/ Aβ1-42 ratios of 10/1 (green curve), 1/1 (orange curves) and 0.25/1 (blue curve; only for TTR). The control curves are represented in red lines and buffer in grey.

Circular dichroism of Aβ1-42 and Aβ1-28. In order to study the influence of **11** on the conformational behavior of Aβ, CD spectra of solution of Aβ1-42 in the absence or presence of the natural peptide **1** and foldamer **11** and recorded at various time points until 5h, showed that **1** and **11** are able to dramatically decrease the parallel β sheet content, confirming that fibrillization kinetics is decreased in the presence of **1** and 11 (Figures S21-23 and full data in SI). Then, in order to better appreciate an early α-helix stabilization of Aβ, we used the 1-28 construct which is non-aggregative and retains the sequence thought to be able to fold into a helix,[58] and demonstrated to have nanomolar affinity with TTR.[33]

However, conducting CD spectra of solution of Aβ1-28 in the absence or presence of **1** or **11**, showed a dramatic effect of **11** to stabilize its α-helical content and to decrease its β-strand content (α-helical / β-strand ratio at 3h: 0.39 for Aβ1-28 alone, 0.66 and 2.16 in the presence of **1** and **11** respectively, Figure S24, SI). This suggests that foldamer **11** is able to interact at the early steps of the kinetics, with the preliminary folding of Aβ before its misfolding in pathological β-sheet structures prone to aggregation. This also indicates that **11** interact with the N-terminal part Aβ1-28 as reported for the EF-helix of TTR.[33]

ThT fluorescence spectroscopy of hIAPP. As it has been very recently shown that TTR can also interfere with the aggregation of another amyloid protein, namely the islet amyloid polypeptide (hIAPP) involved in type 2 Diabetes (T2D),[59,60] the activities on the inhibition of hIAPP aggregation for peptides **1**, **7**, **10** and **11** were also evaluated by ThT fluorescence assay and compared with that of wt-TTR. While we confirmed that wt-TTR delays the aggregation without reducing the fluorescence plateau, the tested peptides showed no effect even at high 10/1 ratio (Figure S20 and Table S16, SI). Thus, the natural peptide **1** and our diazapeptides selectively inhibit Aβ1-42 aggregation. To our knowledge, the nature of the hot-spots of TTR-hIAPP is unknown to date, and our results exclude the EF-helix of TTR in this interaction.

Plasma stability assay. Then, the stability in human plasma of natural peptide **1** and foldamer **11** was compared. Very interestingly, after two hours of incubation at 37 °C, only 6% of our foldamer **11** was degraded whereas 99% of the natural peptide **1** was degraded (Table S18, SI).

BBB permeability and cellular toxicity assays. The BBB permeability of foldamer **11** was thus investigated using *in vitro* rat BBB model (Table S19 and detailed data in SI). No cellular toxicity after 1 h of peptide exposure was observed even at high concentration (100 μg/mL, Figure S25). The apparent permeability (Papp) values of **11** at 10 μM and 5 μM (6.77×10^{-7} and 8.39×10^{-7} cm/s respectively) indicated a limited passage across the *in vitro* rat BBB model. However, this permeability is comparable to that of cell penetrating peptides [61] and higher than that of biologics.[62]

CONCLUSION

A novel class of peptidomimetic foldamers based on diazapeptide units accessible by solid-phase synthesis have shown helical folding properties in water. By studying the impact of the aza substitution in terms of number and position of resi-

dues on the conformation, we showed that the specific incorporation of one diaza-peptide unit at the N- terminus allows the helical folding that is further reinforced by the introduction of a second unit at the C-terminus. The proof of concept for the ability of this new class of foldamers to target PPIs, has been brought by the demonstration that one small helical hotspot of TTR-Aβ interaction can be mimicked to decrease the aggregation of Aβ. This work also demonstrates that: 1- the EF-helix is involved in TTR-Aβ interaction; 2- the novel strategy consisting in mimicking endogenous chaperone proteins by small peptides opens a new way for designing inhibitors of amyloid protein aggregation, the hallmark of more than 20 serious human diseases [24,63]; 3- helical structures of foldamers can stabilize the early helical structures of amyloid proteins, thereby inhibiting the misfolding towards β-sheet rich conformation mediating amyloid aggregation. This feature could also be exploited to target other intrinsically disordered proteins (IDPs), in order to stabilize their helical conformation and promote their interaction with biological partners (folding and binding properties of IDPs).[64] Furthermore, the demonstration that the introduction of a few diaza-peptide units in peptides protects them from the proteolysis and can bring BBB permeability, further confirms that this new class of peptidomimetics present promising future to design PPI inhibitors, ligands of IDPs or other peptide drugs.

EXPERIMENTAL SECTION

Chemistry. Usual solvents were purchased from commercial sources and DCM was dried and distilled over CaH_2. Thin-layer chromatography (TLC) analyses were performed on silica gel 60 F250 (0.26 mm thickness) plates. The plates were visualized with UV light (λ = 254 nm) or stained by a 4 % solution of phosphomolybdic acid or ninhydrin in EtOH. NMR spectra were recorded on an ultrafield Bruker AVANCE 300 (1H, 300 MHz, 13C, 75 MHz) or on a Bruker AVANCE 400 (1H, 400 MHz, 13C, 100 MHz) a Bruker AVANCE I 600 MHz (1H, 600 MHz, 13C, 150 MHz) equipped with a z-gradient TCI. Chemical shifts δ are in ppm with the solvent resonance as the internal standard (1H NMR, $CDCl_3$: δ = 7.26 ppm, DMSO: δ = 2.50 ppm, DMF: δ = 2.75 ppm, CD_3OD and CD_3OH: δ = 3.31 ppm; 13C NMR, $CDCl_3$: δ = 77.16 ppm, DMSO: δ = 39.52 ppm, DMF: δ = 29.76 ppm, CD_3OD and CD_3OH: δ = 49.00 ppm), and the following abbreviations are used: singlet (s), doublet (d), doublet of doublet (dd), triplet (t), multiplet (m), broad multiplet (brm), and broad singlet (brs), broad doublet (brd). Mass spectra were obtained using a Bruker Esquire electrospray ionization apparatus. HRMS were obtained using a TOF LCT Premier apparatus (Waters) with an electrospray ionization source. All the final peptides were purified by semi-preparative HPLC, performed on Agilent 1260 Infinity II. The purity of compounds was determined by HPLC-MS on Agilent 1260 Infinity. Column: Pursuit (C18 10 x 250µm-5µm), mobile phase: ACN/H_2O + 0.1% formic acid. All peptides were >95% pure by HPLC.

Solid phase peptide Synthesis. All the reactions involved were agitated in plastic syringe tubes equipped with filters on an automated shaker. Rink Amide resin (400 mg, 0.4 mmol/g) was swelled by DMF for 1h before using. Each coupling of Fmoc-protected natural amino acids was carried out twice to get satisfactory yields. Removal of Fmoc group was performed in 20%(v/v) piperidine/DMF for 20 min twice. Capping steps were performed by treating with the mixture of acetic anhydride (0.25 M) and NMM (0.25 M) in DMF solution for 20 min. After each reaction, the resin was washed with DMF (3×10mL), MeOH (3×10mL) and DCM (3×10mL) successively. The loading of the first amino acid, Fmoc-Gly-OH (2 equiv), was performed in 20%(v/v) NMM/DMF using HCTU (2 equiv) as coupling reagent for 30 min. Couplings between two natural residues (2 equiv) were also performed in 20%(v/v) NMM/DMF using HCTU (2 equiv) as coupling reagents for 20 min each coupling. To coupling diaza-peptide fragments (compounds **12**, **13**, **14a** and **14b**, see SI) with natural residues, diaza-peptdie fragments (2 equiv) were activated by triphosgene (0.7 equiv) in the presence of DIPEA (2 equiv) in DCM for 15 min (in a flask), then the reactive solutions were transferred to the plastic syringe tubes containing the resin, 3 equiv DIPEA was added and the reactions were agitated at room temperature for 5 h. To coupling natural amino acids to aza-residues, the natural amino aicds (2 equiv) were firstly activated by DIC (2 equiv) and Oxyma (3.3 equiv) in the mixture of DCM/DMF (1/1) (8 mL) for 10 min (in a flask), then the solutions were transferred to the plastic syringe tubes containing the resin, 15 equiv collidine was added as base. For the coupling Lys to aza-Leu residue, the reaction was agitated at room temperature for 5 h. For the coupling Ser to aza-Tyr residue, the reaction was agitated at 40°C for 5 h.

Circular Dichroism Spectroscopy. Peptides were dissolved in MQ water to a concentration of 750 µM as stock solutions. For the measurement in 20 mM PB solution, 50 µL of stock solution was taken into a cuvette with a pathlength of 1 mm, then the solution was diluted by 250 µL PB solution to a final concentration of 125 µM. The CD spectra were measured by Jasco J-810 spectropolarimeter from 190 to 260 nm at corresponding temperature. For the measurement in methanol, 50 µL of stock solution in a cuvette was diluted by 250 µL methanol to a final concentration of 125 µM. The CD spectra were recorded from 195 to 260 nm at corresponding temperature. For the measurement in $CaCl_2$ aqueous solution or urea aqueous solution, 50 µL of stock solution in a cuvette was diluted by 250 µL 1 M $CaCl_2$ aqueous solution or 6 M urea aqueous solution to a final concentration of 125 µM. The CD spectra were recorded from 210 to 260 nm at corresponding temperature. Each CD spectrum was corrected by subtracting the corresponding baseline (50 µL MQ water + 250 µL corresponding diluent).

FT - IR Spectroscopy. Infrared spectra were recorded using a Shimadzu IRAffinity-1S spectrometer in the range 600–4000 cm^{-1} with a resolution of 2 cm^{-1}. A sample for measurements in the solid state was prepared by dissolving the peptidomimetic in H_2O and MeOH, placing the solution on the crystal plate, and evaporating the solvent (64 scans were averaged). The ATR FT-IR experiment were measured from a solution at 2 mM compound concentration. Transmittance has been recorded and transformed into absorbance (A = 2-log(T)). Data processing was performed using Solver in Excel software (Microsoft). Deconvolution of the spectra was done in the spectral range 1500 - 1800 cm–1. The deconvoluted spectra were fitted with Gaussian band profiles. The positions, and number of the components, which were used as an input file for the curve-fitting function, were obtained from the deconvoluted spectra. The quality of the fitting was estimated by standard deviation and error squared.

MD simulations in explicit water. Initial three-dimensional structures of compounds **7** and **11** were generated using the program MarvinSketch 6.2.1 from ChemAxon (https://www.chemaxon.com). Each molecule was placed in a

cubic simulation box so that the minimum distance between the solute and the cube sides was 1.4 nm. Simulation boxes were filled with TIP3P water molecules and 2 or 3 chloride ions to neutralize compound 7 or 11, respectively. MD simulations were performed using the GROMACS 2019.1 package[65] with the Generalized AMBER Force Field (GAFF)[66] for both solutes. Covalent bonds involving hydrogens were kept rigid using the LINCS procedure.[67] Lennard-Jones potentials were cut-off at 1.2 nm and electrostatic interactions were treated using the smooth PME method.[68] After two short simulations of 1 ns each to equilibrate the system temperature and pressure around T = 300 K and P = 1 bar, each compound was simulated during 500 ns in the isothermal-isobaric (NPT) ensemble using the Nose-Hoover and Parrinello-Rahman coupling methods. Molecular coordinates were saved every 20 ps for subsequent analyses by the GROMACS tools gmx mindist for calculating interproton distances and gmx angle for extracting torsion angle values. $^3J_{NH\text{-}H\alpha}$ coupling constants were computed from the backbone ϕ dihedral angles by using the Karplus equation with the parameters A=6.51, B=-1.76, and C=1.60. Conformational ensembles were clustered using the *gromos* method implemented in *gmx* cluster.

Fluorescence-Detected ThT Binding Assay (Aβ1–42). Aβ1–42 was purchased from Bachem and ThT was obtained from Sigma. The peptide was dissolved in an aqueous 1% ammonia solution to a concentration of 1 mM and then, just prior to use, was diluted to 0.2 mM with 10 mM Tris-HCl and 100 mM NaCl buffer (pH 7.4). Stock solutions of compounds to test were dissolved in water. Lyophilized prealbumin, human plasma (wt-TTR as tetramer) was purchased from Merck Millipore (Molsheim, France). ThT fluorescence was measured to evaluate the development of Aβ1–42 fibrils over time using a fluorescence plate reader (Fluostar Optima, BmgLabtech) with standard 96-well black microtiter plates (final volume in the wells of 200 µL). Experiments were started by adding the peptide (final Aβ1–42 concentration equal to 10 µM) into a mixture containing 40 µM ThT in 10 mM Tris-HCl and 100 mM NaCl buffer (pH 7.4) with and without the compounds at different concentrations (100 and 10 µM) at room temperature. The ThT fluorescence intensity of each sample (performed in triplicate) was recorded with 440/480 nm excitation/emission filters set for 42 h performing a double orbital shaking of 10 s before the first cycle. The fluorescence assays were performed between 2 and 4 times on different days, with the same batch of peptide. The ability of compounds to inhibit Aβ1–42 aggregation was assessed considering the time of the half-aggregation (t1/2) and the intensity of the experimental fluorescence plateau (F), both values were obtained by fitting the obtained kinetic data to a Boltzmann sigmoidal curve using GraphPad Prism 5. The relative extension of $t_{1/2}$ is defined as the experimental $t_{1/2}$ in the presence of the tested compound relative to the one obtained without the compound and is evaluated as the following percentage: [$t_{1/2}$ (Aβ + compound) – $t_{1/2}$ (Aβ)] / $t_{1/2}$ (Aβ) × 100. The relative extension/reduction of the experimental plateau is defined as the intensity of experimental fluorescence plateau observed with the tested compound relative to the value obtained without the compound and is evaluated as the following percentage: (Faβ + compound – Faβ) / Faβ × 100. Curves of the tested compounds are fitted to a Boltzmann sigmoidal model, normalized to the control experiment.

Circular dichroism analysis of Aβ1-42 and Aβ1-28. CD spectra (195-250 nm) were acquired on Jasco J-810 using 0.1 cm quartz cells. The spectra were recorded with 0.1 nm resolution at 25°C and a scan rate of 50 nm/min. Five scans were acquired and averaged for each sample (Aβ1-42 or Aβ1-28 at 25 µM concentration and inhibitor at 125 µM). The data are given as CD intensity in mdeg. Raw data were processed by background subtraction (or inhibitor subtraction when required), followed by smoothing. Secondary structure percentages were calculated from these spectra over the range 200-250 nm using the freely accessible algorithm BeStSel (best-sel.elte.hu) which includes independent basis spectra for both parallel and antiparallel β-sheet. The deconvolution was performed on the CD measurement, after subtraction of the corresponding buffer or the solution containing the 125 µM concentration of inhibitor.

Human Plasmatic Stability Study. Human plasma was obtained from Etablissement Français du Sang (EFS, Les Ulis, France). Compounds were incubated in duplicate at 1 µM in plasma at 37°C from 0 to 120 minutes (T0, 15, 30, 45, 60 and 120 min). At each time points, 200 µL of acetonitrile was added to 50 µL of incubated plasma. After vortexing 10 seconds and centrifugation 10 minutes at 20000g, supernatant was evaporated to dryness under nitrogen stream 1 hour at 40°C and the dry extract was reconstituted with 50 µL water/acetonitrile (90/10; v/v). After centrifugation 5 minutes at 20000g supernatant was transferred into a vial placed at 4°C in the autosampler before injection into the analytical system. Compounds quantitation was carried out using an UPLC–MS/MS system consisted of a Waters ACQUITY UPLC® System coupled to a Waters XEVO™ TQ-S Mass Spectrometer operating in positive ion electrospray MRM mode. Reversed phase analysis was performed with an Acquity UPLC BEH C18 1.7 µm, 2.1x50 mm column maintained at 40°C and a gradient over a run time of 4 minutes. All solvents and chemicals were of LC/MS grade and were purchased from VWR International. Mobile phase A was 0.1% formic acid in water and mobile phase B 0.1% formic acid in acetonitrile.

Blood-Brain Barrier (BBB) Permeability Measurement. The study consisted of measuring the passage of compound **11** through in vitro rat blood-brain barrier (BBB) model. The integrity and functionality of in vitro rat BBB model were assessed by monitoring the transport of 3 molecules: Lucifer Yellow (LY), propranolol and vinblastine. In addition, compound **11** was co-incubated with LY, which served as the internal integrity standard. Compound **11** was tested at 5 µM and 10 µM. The solutions were prepared in low-binding Eppendorf tubes to limit the loss of compound **11**. By so doing, the concentrations measured in the To solutions were closer the target concentration of 5 and 10 µM. The study was performed on rat BBB model in the apical-to-basal direction (i.e. blood to brain) and from the basal to apical concentration in triplicate. The samples obtained from the apical and basal compartments were then analyzed using a developed analytical LC-MS/MS method, thus making it possible to establish the rate of passage of compound **11**. The apparent permeability (Papp) values of **11** at 10 µM and 5 µM (6.77x10-7 cm/s and 8.39 x10-7 cm/s respectively) were lower than that of Lucifer yellow, a reference compound (3.13x10-6 cm/s), indicating a limited passage across the in vitro rat BBB model. The differences of ratios between the apparent permeability values of the peptide at 5µM and from the basal to apical compartment and from the apical to basal compartment about 2.6 suggest that **11** is a potential substrate of the efflux transporters located at the rat BBB, explaining its low permeability.

ASSOCIATED CONTENT

Supporting Information. All the experimental procedures, and complete data for the synthesis protocols, compounds characterization, CD, FT-IR, MD simulations, ThT Fluorescence, Amylofit, human plasma stability, cellular toxicity and BBB permeability are provided in the Supporting Information (supporting information JMedChem_SHI_ONGERI.docx).
Superposition of compounds 7 and 11 with TTR helix:
Superposition_Fold7_EFhelix.avi
Superposition_Fold11_EFhelix.avi
Molecular formula String : SMILES-JMedChem.csv

AUTHOR INFORMATION

Corresponding Authors

* **Dr. Nicolo Tonali** - *Université Paris-Saclay, CNRS, BioCIS, Bat. Henri Moissan, 17 av. des Sciences, 91400 Orsay, France,* E-mail: nicolo.tonali@universite-paris-saclay.fr
ORCID: https://orcid.org/0000-0002-1435-5676

* **Prof. Dr. Sandrine Ongeri** - *Université Paris-Saclay, CNRS, BioCIS, Bat. Henri Moissan, 17 av. des Sciences, 91400 Orsay, France,* E-mail: sandrine.ongeri@universite-paris-saclay.fr
ORCID: https://orcid.org/0000-0002-2118-7324

Author Contributions

The manuscript was written through contributions of all authors. All authors have given approval to the final version of the manuscript.

Notes

The authors declare no competing financial interest.

ACKNOWLEDGMENTS

Karine Leblanc (Service d'Analyses–HPLC-Masse BioCIS, Univ. Paris Saclay) is thanked for HPLC and HRMS analyses. The China Scholarship Council (CSC) is thanked for the PhD fellowships for C. Shi.

ABBREVIATIONS USED

Aβ, amyloid β; ACN, acetonitrile; AD, Alzheimer's disease; Ala, alanine; ATR-FTIR, attenuated total reflectance-Fourier transform infrared spectroscopy; BBB, blood-brain barrier; CD, circular dichroism; Boc, tert-butyloxycarbonyle; CSF, cerebrospinal fluid; DIC, N,N-diisopropylcarbodiimide; DIPEA, N, N-diisopropylethylamine; DMF, dimethylformamide; Fmoc, fluorenylmethyloxycarbonyl; HCTU, 2-(6-Chloro-1-H-benzotriazole-1-yl)-1,1,3,3-tetramethylaminium hexafluorophosphate; hIAPP, human islet amyloid polypeptide; IDP, intrinsically disordered protein; kDa, kilodalton; Leu, leucine; Lys, lysine; MD, molecular dynamics; NMM, N-methylmorpholine; NMR, nuclear magnetic resonance; PB, phosphate buffer; PDB, protein databank; PPI, protein-protein interaction; RMSD, root-mean-square deviation; ROE, rotating-frame Overhauser effect; SPPS, solid-phase peptide synthesis; ThT, Thioflavin-T; TBDMS, tert-butyldimethylsilyl; TFA, trifluoroacetic acid; Thr, threonine; TIPS, triisopropylsilyl; Trp, tryptophane; TTR, transthyretin; Tyr, tyrosine

REFERENCES

(1) H. Lu, Q. Zhou, J. He, Z. Jiang, C. Peng, R. Tong, J. Shi, Recent advances in the development of protein-protein interactions modulators: mechanisms and clinical trials. *Signal Transduct. Target. Ther.* **2020**, 5, 1–23.

(2) X. Ran, J. E. Gestwicki, Inhibitors of protein-protein interactions (PPIs): an analysis of scaffold choices and buried surface area. *Curr. Opin. Chem. Biol.* **2018**, 44, 75–86.

(3) E. Martino, S. Chiarugi, F. Margheriti, G. Garau, Mapping, Structure and Modulation of PPI. *Front. Chem.* **2021**, 9, 718405.

(4) H. Bruzzoni-Giovanelli, V. Alezra, N. Wolff, C.-Z. Dong, P. Tuffery, A. Rebollo, Interfering peptides targeting protein-protein interactions: the next generation of drugs? *Drug Discov.* **2018**, 23, 272–285.

(5) M. Pelay-Gimeno, A. Glas, O. Koch, T. N. Grossmann, Structure-Based Design of Inhibitors of Protein-Protein Interactions: Mimicking Peptide Binding Epitopes. *Angew. Chem. Int. Ed.* **2015**, 54, 8896–8927.

(6) J. Laxio Arenas, J. Kaffy, S. Ongeri, Peptides and peptidomimetics as inhibitors of protein-protein interactions involving β-sheet secondary structures. *Curr. Opin. Chem. Biol.* **2019**, 52, 157–167.

(7) R. Gopalakrishnan, A. I. Frolov, L. Knerr, W. J. Drury, E. Valeur, Therapeutic Potential of Foldamers: From Chemical Biology Tools To Drug Candidates? *J. Med. Chem.* **2016**, 59, 9599–9621.

(8) I. M. Mándity, F. Fülöp, An overview of peptide and peptoid foldamers in medicinal chemistry. *Expert Opin. Drug Discov.* **2015**, 10, 1163–1177.

(9) G. Olajos, É. Bartus, I. Schuster, G. Lautner, R. E. Gyurcsányi, T. Szögi, L. Fülöp, T. A. Martinek, Multivalent foldamer-based affinity assay for selective recognition of Aβ oligomers. *Anal. Chim. Acta*, **2017**, *960*, 131-137.

(10) W. S. Horne, L. M. Johnson, T. J. Ketas, P. J. Klasse, M. Lu, J. P. Moore, S. H. Gellman, Structural and biological mimicry of protein surface recognition by alpha/beta-peptide foldamers. *Proc. Natl. Acad. Sci.* **2009**, 106, 14751–14756.

(11) L. Cussol, L. Mauran-Ambrosino, J. Buratto, A. Y. Belorusova, M. Neuville, J. Osz, S. Fribourg, J. Fremaux, C. Dolain, S. R. Goudreau, N. Rochel, G. Guichard, Structural Basis for α-Helix Mimicry and Inhibition of Protein-Protein Interactions with Oligourea Foldamers. *Angew. Chem. Int. Ed.* **2021**, 60, 2296–2303.

(12) A. Begum, S. Dodoala, K. Prasad, B. Koganti, A Review on Azapeptides: The Promising Peptidomimetics. *Asian J. Chem.* **2017**, 29, 1879–1887.

(13) C. Proulx, D. Sabatino, R. Hopewell, J. Spiegel, Y. García Ramos, W. D. Lubell, Azapeptides and their therapeutic potential. *Future Med Chem* **2011**, 3, 1139–1164.

(14) K. Tarchoun, M. Yousef, Z. Bánóczi, Azapeptides as an Efficient Tool to Improve the Activity of Biologically Effective Peptides. *Future Pharmacol.* **2022**, 2, 293–305.

(15) R. Chingle, C. Proulx, W. D. Lubell, Azapeptide Synthesis Methods for Expanding Side-Chain Diversity for Biomedical Applications. *Acc. Chem. Res.* **2017**, 50, 1541–1556.

(16) A. Altiti, M. He, S. VanPatten, K. F. Cheng, U. Ahmed, P. Y. Chiu, I. T. Mughrabi, B. Al Jabari, R. M. Burch, K. R. Manogue, K. J. Tracey, B. Diamond, C. N. Metz, H. Yang, L. K. Hudson, S. Zanos, M Son, B. Sherry, T. R. Coleman, Y. Al-Abed. Thiocarbazate building blocks enable the construction of azapeptides for rapid development of therapeutic candidates. *Nat Commun* **2022**, 13, 7127.

(17) F. Bizet, N. Tonali, J.-L. Soulier, A. Oliva, J. Kaffy, B. Crousse, S. Ongeri, Towards a general synthesis of di-aza-amino acids containing peptides. *New J. Chem.* **2018**, 42, 17062–17072.

(18) N. Tonali, I. Correia, J. Lesma, G. Bernadat, S. Ongeri, O. Lequin, Introducing sequential aza-amino acids units induces repeated β-turns and helical conformations in peptides. *Org. Biomol. Chem.* **2020**, 18, 3452–3458.

(19) C. Shi, I. Correia, N. Tonali, S. Ongeri, O. Lequin, Two consecutive aza-amino acids in peptides promote stable β-turn formation in water. *Org. Biomol. Chem.* **2022**, 20, 8430-8437.

(20) T. Gião, J. Saavedra, E. Cotrina, J. Quintana, J. Llop, G. Arsequell, I. Cardoso, Undiscovered Roles for Transthyretin: From a Transporter Protein to a New Therapeutic Target for Alzheimer's Disease. *Int. J. Mol. Sci.* **2020**, 21, 2075.

(21) N. N. Nalivaeva, A. J. Turner, Br. Targeting amyloid clearance in Alzheimer's disease as a therapeutic strategy. *J. Pharmacol.* **2019**, 176, 3447–3463.

(22) L. C. dos S. Picanco, P. F. Ozela, M. de F. de B. Brito, A. A. Pinheiro, E. C. Padilha, F. S. Braga, C. H. T. de P. da Silva, C. B. R. dos Santos, J. M. C. Rosa, L. I. da S. Hage-Melim, Alzheimer's Disease: A Review from the Pathophysiology to Diagnosis, New Perspectives for Pharmacological Treatment. *Curr. Med. Chem.* **2018**, 25, 3141–3159.

(23) D. S. Knopman, H. Amieva, R. C. Petersen, G. Chételat, D. M. Holtzman, B. T. Hyman, R. A. Nixon, D. T. Jones Alzheimer disease. *Nat. Rev. Dis. Primers* **2021**, 7, 33.

(24) P. H. Nguyen, A. Ramamoorthy, B. R. Sahoo, J. Zheng, P. Faller, J. E. Straub, L. Dominguez, J. E. Shea, N. V. Dokholyan, A. De Simone, B. Ma, R. Nussinov, S. Najafi, S. T. Ngo , A. Loquet, M. Chiricotto, P. Ganguly, J. McCarty, M. S. Li, C. Hall, Y. Wang, Y. Miller, S. Melchionna, B. Habenstein, S. Timr, J. Chen, B. Hnath , B. Strodel, R. Kayed, S. Lesné, G. Wei, F. Sterpone, A. J. Doig, P. Derreumaux, Amyloid Oligomers: A Joint Experimental/Computational Perspective on Alzheimer's Disease, Parkinson's Disease, Type II Diabetes, and Amyotrophic Lateral Sclerosis. *Chem Rev.* **2021**, *121*, 2545-2647.

(25) S. H. Choi, S. N. Leight, V. M.-Y. Lee, T. Li, P. C. Wong, J. A. Johnson, M. J. Saraiva, S. S. Sisodia, Accelerated Aβ Deposition in APPswe/PS1ΔE9 Mice with Hemizygous Deletions of TTR (Transthyretin). *J. Neurosci.* **2007**, 27, 7006–7010.

(26) J. N. Buxbaum, Z. Ye, N. Reixach, L. Friske, C. Levy, P. Das, T. Golde, E. Masliah, A. R. Roberts, T. Bartfai, Transthyretin protects Alzheimer's mice from the behavioral and biochemical effects of Abeta toxicity. *Proc. Natl. Acad. Sci.* **2008**, 105, 2681–2686.

(27) S.-H. Han, E. S. Jung, J.-H. Sohn, H. J. Hong, H. S. Hong, J. W. Kim, D. L. Na, M. Kim, H. Kim, H. J. Ha, Y. H. Kim, N. Huh, M. W. Jung, I. Mook-Jung, Human Serum Transthyretin Levels Correlate Inversely with Alzheimer's Disease. *J. Alzheimer's Dis.* **2011**, 25, 77–84.

(28) J.-M. Serot, D. Christmann, T. Dubost, M. Couturier, Cerebrospinal fluid transthyretin: aging and late onset Alzheimer's disease. *J. Neurol. Neurosurg. Psychiatry* **1997**, 63, 506–508.

(29) P. Y. Cho, G. Joshi, J. A. Johnson, R. M. Murphy, Transthyretin-Derived Peptides as β-Amyloid Inhibitors. *ACS Chem. Neurosci.* **2014**, 5, 542–551.

(30) P. Y. Cho, G. Joshi, M. D. Boersma, J. A. Johnson, R. M. Murphy, A Cyclic Peptide Mimic of the β-Amyloid Binding Domain on Transthyretin. *ACS Chem. Neurosci.* **2015**, 6, 778–789.

(31) X. Lu, C. R. Brickson, R. M. Murphy, TANGO-Inspired Design of Anti-Amyloid Cyclic Peptides. AC*S Chem. Neurosci.* **2016**, 7, 1264–1274.

(32) K. M. Pate, B. J. Kim, E. V. Shusta, R. M. Murphy, Transthyretin Mimetics as Anti-β-Amyloid Agents: A Comparison of Peptide and Protein Approaches. *ChemMedChem* **2018**, 13, 968–979.

(33) L. Ciccone, C. Fruchart-Gaillard, G. Mourier, M. Savko, S. Nencetti, E. Orlandini, D. Servent, E. A. Stura, W. Shepard, Copper mediated amyloid-β binding to Transthyretin. *Sci Rep.* **2018**, 8, 13744.

(34) D. Boeglin, W. D. Lubell, Aza-Amino Acid Scanning of Secondary Structure Suited for Solid-Phase Peptide Synthesis with Fmoc Chemistry and Aza-Amino Acids with Heteroatomic Side Chains. *J. Comb. Chem.* **2005**, 7, 864–878.

(35) C. Proulx, W. D. Lubell, N-Amino-imidazolin-2-one Peptide Mimic Synthesis and Conformational Analysis. *Org. Lett.* **2010**, 12, 2916–2919.

(36) C. M. Grison, S. Robin, D. J. Aitken, 13-Helix folding of a β/γ-peptide manifold designed from a "minimal-constraint" blueprint. *Chem. Commun*. **2016**, 52, 7802–7805.

(37) C. M. Grison, J. A. Miles, S. Robin, A. J. Wilson, D. J. Aitken, An α-Helix-Mimicking 12,13-Helix: Designed α/β/γ-Foldamers as Selective Inhibitors of Protein–Protein Interactions. *Angew. Chem. Int. Ed.* **2016**, 55, 11096–11100.

(38) L. Bodero, K. Guitot, N. Lensen, O. Lequin, T. Brigaud, S. Ongeri, G. Chaume, Introducing the Chiral Constrained α-Trifluoromethylalanine in Aib Foldamers to Control, Quantify and Assign the Helical Screw-Sense. *Chem. Eur. J.* **2022**, 28, e202103887.

(39) C. Toniolo, A. Polese, F. Formaggio, M. Crisma, J. Kamphuis, Circular Dichroism Spectrum of a Peptide 310-Helix. *J. Am. Chem. Soc.* **1996**, 118, 2744–2745.

(40) W. A. Elam, T. P. Schrank, A. J. Campagnolo, V. J. Hilser, Evolutionary conservation of the polyproline II conformation surrounding intrinsically disordered phosphorylation sites. *Biochem.* **2013**, 52, 949–958.

(41) J. Kapitán, D. Gallo, N. Goasdoué, M. Nicaise, M. Desmadril, L. Hecht, G. Leclercq, L. D. Barron, Y. Jacquot, Identification of a human estrogen receptor α-derived anti-estrogenic peptide that adopts a polyproline II conformation. J. *Pept. Sci.* **2009**, 15, 455–464.

(42) A. G. Cochran, N. J. Skelton, M. A. Starovasnik, Tryptophan zippers: stable, monomeric beta –hairpins. *Proc. Natl. Acad. Sci.* **2001**, 98, 5578–5583.

(43) L. Wu, D. McElheny, T. Takekiyo, T. A. Keiderling, Geometry and Efficacy of Cross-Strand Trp/Trp, Trp/Tyr, and Tyr/Tyr Aromatic Interaction in a β-Hairpin Peptide. *Biochem.* **2010**, 49, 4705–4714.

(44) W. K. Surewicz, H. H. Mantsch, D. Chapman, Determination of protein secondary structure by Fourier transform infrared spectroscopy: a critical assessment. *Biochem.* **1993**, 32, 389–394.

(45) H. Yang, S. Yang, J. Kong, A. Dong, S. Yu, Obtaining information about protein secondary structures in aqueous solution using Fourier transform IR spectroscopy. *Nat. Protoc.* **2015**, 10, 382–396.

(46) L. J. Smith, K. A. Bolin, H. Schwalbe, M. W. MacArthur, J. M. Thornton, C. M. Dobson, Analysis of main chain

torsion angles in proteins: prediction of NMR coupling constants for native and random coil conformations. *J. Mol. Biol.* **1996**, 255, 494–506.

(47) F. Avbelj, S. G. Grdadolnik, J. Grdadolnik, R. L. Baldwin, Intrinsic backbone preferences are fully present in blocked amino acids. *Proc. Natl. Acad. Sci.* **2006**, 103, 1272–1277.

(48) S. M. Gagné, S. Tsuda, M. X. Li, M. Chandra, L. B. Smillie, B. D. Sykes, Quantification of the calcium-induced secondary structural changes in the regulatory domain of troponin-C. *Protein Sci.* **1994**, 3, 1961–1974.

(49) A. S. Maltsev, A. Grishaev, A. Bax, Monomeric α-Synuclein Binds Congo Red Micelles in a Disordered Manner. *Biochem.* **2012**, 51, 631–642.

(50) H. LeVine, Quantification of beta-sheet amyloid fibril structures with thioflavin T. *Methods in Enzymology, Academic Press*, **1999**, pp. 274–284.

(51) K. Gade Malmos, L. M. Blancas-Mejia, B. Weber, J. Buchner, M. Ramirez-Alvarado, H. Naiki, D. Otzen, ThT 101: a primer on the use of thioflavin T to investigate amyloid formation. *Amyloid* **2017**, 24, 1–16.

(52) J. Kaffy, C. Berardet, L. Mathieu, B. Legrand, M. Taverna, F. Halgand, G. Van Der Rest, L. T. Maillard, S. Ongeri, Helical γ-Peptide Foldamers as Dual Inhibitors of Amyloid-β Peptide and Islet Amyloid Polypeptide Oligomerization and Fibrillization. *Chem. Eur. J.* **2020**, 26, 14612–14622.

(53) S. Pellegrino, N. Tonali, E. Erba, J. Kaffy, M. Taverna, A. Contini, M. Taylor, D. Allsop, M. L. Gelmi, S. Ongeri, β-Hairpin mimics containing a piperidine–pyrrolidine scaffold modulate the β-amyloid aggregation process preserving the monomer species. *Chem. Sci.* **2017**, 8, 1295–1302.

(54) J. Kaffy, D. Brinet, J.-L. Soulier, I. Correia, N. Tonali, K. F. Fera, Y. Iacone, A. R. F. Hoffmann, L. Khemtémourian, B. Crousse, M. Taylor, D. Allsop, M. Taverna, O. Lequin, S. Ongeri, Designed Glycopeptidomimetics Disrupt Protein–Protein Interactions Mediating Amyloid β-Peptide Aggregation and Restore Neuroblastoma Cell Viability. *J. Med. Chem.* **2016**, 59, 2025–2040.

(55) L. Vahdati, J. Kaffy, D. Brinet, G. Bernadat, I. Correia, S. Panzeri, R. Fanelli, O. Lequin, M. Taverna, S. Ongeri, U. Piarulli, Synthesis and Characterization of Hairpin Mimics that Modulate the Early Oligomerization and Fibrillization of Amyloid β-Peptide. *Eur. J. Org. Chem.* **2017**, 2017, 2971–2980.

(56) G. Meisl, J. B. Kirkegaard, P. Arosio, T. C. T. Michaels, M. Vendruscolo, C. M. Dobson, S. Linse, T. P. J. Knowles, Molecular mechanisms of protein aggregation from global fitting of kinetic models. *Nat. Protoc.* **2016**, 11, 252–272.

(57) https://amylofit.com

(58) A. Santoro, M. Grimaldi, M. Buonocore, I. Stillitano, A. M. D'Ursi, Exploring the Early Stages of the Amyloid Aβ(1-42) Peptide Aggregation Process: An NMR Study. Pharmaceuticals (Basel). 2021 Jul 27;14(8):732.

(59) S. Wasana Jayaweera, S. Surano, N. Pettersson, E. Oskarsson, L. Lettius, A. L. Gharibyan, I. Anan, A. Olofsson, Mechanisms of Transthyretin Inhibition of IAPP Amyloid Formation. *Biomolecules* **2021**, 11, 411.

(60) D. Milardi, E. Gazit, S. E. Radford, Y. Xu, R. U. Gallardo, A. Caflisch, G. T. Westermark, P. Westermark, C. Rosa, A. Ramamoorthy. Proteostasis of Islet Amyloid Polypeptide: A Molecular Perspective of Risk Factors and Protective Strategies for Type II Diabetes. *Chem Rev.* **2021**, 121, 1845-1893.

(61) P. Majerova, J. Hanes, D. Olesova, J. Sinsky, E. Pilipcinec, A. Kovac, Novel Blood–Brain Barrier Shuttle Peptides Discovered through the Phage Display Method. *Molecules* **2020**, 25, 874.

(62) W. M. Pardridge, Treatment of Alzheimer's Disease and Blood-Brain Barrier Drug Delivery. *Pharmaceuticals (Basel)* **2020**, 13, 394.

(63) P. C. Ke, M.-A. Sani, F. Ding, A. Kakinen, I. Javed, F. Separovic, T. P. Davis and R. Mezzenga, Implications of peptide assemblies in amyloid diseases. *Chem. Soc. Rev.* **2017**, 46, 6492–6531.

(64) P. Kulkarni, S. Bhattacharya, S. Achuthan, A. Behal, M. K. Jolly, S. Kotnala, A. Mohanty, G. Rangarajan, R. Salgia, V. Uversky, Intrinsically Disordered Proteins: Critical Components of the Wetware. *Chem. Rev.* **2022**, 122, 6614–6633.

(65) M. J. Abraham, T. Murtola, R. Schulz, S. Páll, J. C. Smith, B. Hess, E. Lindahl, GROMACS: High performance molecular simulations through multi-level parallelism from laptops to supercomputers. *SoftwareX* **2015**, 1–2, 19–25.

(66) J. Wang, R. M. Wolf, J. W. Caldwell, P. A. Kollman, D. A. Case, Development and testing of a general amber force field. *J. Comput. Chem.* **2004**, 25, 1157–1174.

(67) B. Hess. P-LINCS: A Parallel Linear Constraint Solver for Molecular Simulation, *J. Chem. Theory Comput.* **2008**, *4*, 116-122.

(68) U. Essmann, L. Perera, M.L. Berkowitz, T. Darden, H. Lee, L.G. Pedersen. A smooth particle mesh Ewald method, *J. Chem. Phys.* **1995**, *103*, 8577–8593.

Table of Contents artwork